HHS Public Access

Author manuscript

Biomaterials. Author manuscript; available in PMC 2015 August 01.

Published in final edited form as:

Biomaterials. 2014 August ; 35(25): 6838–6849. doi:10.1016/j.biomaterials.2014.04.115.

Macrophage polarization in response to ECM coated polypropylene mesh

MT Wolf[1,3], **CL Dearth**[2,3], **CA Ranallo**[1,3], **S LoPresti**[1,3], **LE Carey**[1,3], **KA Daly**[2,3], **BN Brown**[1,3], and **SF Badylak**[1,2,3,*]

[1] Department of Bioengineering, University of Pittsburgh, Pittsburgh, PA

[2] Department of Surgery, University of Pittsburgh, Pittsburgh, PA

[3] McGowan Institute for Regenerative Medicine, University of Pittsburgh, Pittsburgh, PA

Abstract

The host response to implanted biomaterials is a highly regulated process that influences device functionality and clinical outcome. Non-degradable biomaterials, such as knitted polypropylene mesh, frequently elicit a chronic foreign body reaction with resultant fibrosis. Previous studies have shown that an extracellular matrix (ECM) hydrogel coating of polypropylene mesh reduces the intensity of the foreign body reaction, though the mode of action is unknown. Macrophage participation plays a key role in the development of the foreign body reaction to biomaterials, and therefore the present study investigated macrophage polarization following mesh implantation. Spatiotemporal analysis of macrophage polarization was conducted in response to uncoated polypropylene mesh and mesh coated with hydrated and dry forms of ECM hydrogels derived from either dermis or urinary bladder. Pro-inflammatory M1 macrophages (CD86+/CD68+), alternatively activated M2 macrophages (CD206+/CD68+), and foreign body giant cells were quantified between 3-35 days. Uncoated polypropylene mesh elicited a dominant M1 response at the mesh fiber surface, which was decreased by each ECM coating type beginning at 7 days. The diminished M1 response was accompanied by a reduction in the number of foreign body giant cells at 14 and 35 days, though there was a minimal effect upon the number of M2 macrophages at any time. These results show that ECM coatings attenuate the M1 macrophage response and increase the M2/M1 ratio to polypropylene mesh *in vivo*.

1. Introduction

The host response to surgically implanted biomaterials and medical devices is a complex, temporally regulated process and a critical determinant of success or failure. The host tissue

* Corresponding author. All correspondence should be addressed to: Stephen F. Badylak, 450 Technology Drive, Suite 300, University of Pittsburgh, Pittsburgh, PA 15219, USA, Phone: 412-624-5253; Fax: 412-624-5256; badylaks@upmc.edu.

response to any implanted device generally occurs through interactions at the host-material surface. Non-degradable synthetic polymers used for long term implantation, such as polytetrafluoroethylene (PTFE), polyethylene terephthalate, and polypropylene provide strong reinforcement for surgical repair of soft tissues and confer consistent material properties [1-3]. However, these non-degradable materials elicit a classic foreign body reaction following implantation. The foreign body reaction has been well characterized from a histopathologic perspective, and components of the innate immune response, notably macrophages, rapidly accumulate at the biomaterial surface and play a determinant role in outcomes [4-6]. Inability of macrophages to eliminate a non-degradable or slowly degradable material results in chronic inflammation and a mature foreign body reaction. Macrophage fusion into multinucleate foreign body giant cells and eventual fibrotic scar tissue deposition are hallmarks of this response [4, 7].

The gold standard for biomaterials used in ventral hernia repair is the use of a synthetic polymer, notably knitted polypropylene surgical mesh [8]. Polypropylene is non-degradable, and the inevitable foreign body reaction is typically associated with fibrosis, decreased tissue compliance, and low grade localized chronic inflammation. These sequelae may result in patient discomfort, increased morbidity, and/or mesh explantation [9, 10]. In contrast, surgical mesh materials composed of naturally occurring extracellular matrix (ECM) typically facilitate a constructive host response in which site appropriate host tissue is formed with minimal fibrosis [11-13], but are less mechanically robust and have more variable composition than their synthetic counterparts [14, 15]. ECM scaffolds are prepared by decellularization of various mammalian tissues including, but not limited to, dermis, small intestinal submucosa, pericardium, and urinary bladder [13]. The mechanisms of ECM scaffold remodeling are only partially understood, but modulation of the innate immune response is a critical determinant of the downstream structural and functional outcome. A method was recently described by which a hydrogel form of dermal ECM was used as a coating for a polypropylene hernia mesh, with an associated reduction in the intensity of the foreign body reaction, reduced number of foreign body giant cells, and the diminished density of host deposited collagen during the initial 35 days of *in vivo* implantation [16]. However, the mechanisms of this abrogated host response were not investigated.

The innate immune response to an implanted ECM scaffold is characterized by a transient neutrophil accumulation [17, 18] followed by a sustained and robust accumulation of macrophages within and around the implanted ECM [18-21]. Thus at early time points, the histomorphology is similar to the cellular response to synthetic materials. However, the final outcomes of ECM and non-degradable synthetic materials are markedly different. A potential cause of the disparate host response is the macrophage phenotype elicited by the respective biomaterials. Macrophages may be polarized along a spectrum between two contrasting functional phenotypes: the classically activated pro-inflammatory M1 phenotype associated with host defense and the foreign body reaction vs. the alternatively activated M2 phenotype associated with constructive tissue remodeling [22, 23]. Macrophages involved in constructive tissue remodeling facilitated by biologic scaffold materials show a greater proportion of the M2 phenotype compared to the dominant M1 phenotypic profile observed in the presence of non-degradable synthetic materials or chemically crosslinked, slowly

degradable ECM [19, 20, 24]. The objective of the present study was to determine the effect of an ECM hydrogel coating on the spatiotemporal macrophage polarization response to polypropylene mesh in a rodent model of body wall injury.

2. Materials & Methods

2.1. Overview of experimental design

The spatiotemporal macrophage phenotype response to polypropylene mesh, with and without an ECM hydrogel coating, was evaluated *in vivo*. Dermal and urinary bladder tissues were decellularized to create D-ECM and UBM-ECM scaffolds, respectively. These ECM biomaterials were applied as ECM hydrogel coatings, in hydrated or dried states, to a heavy-weight polypropylene mesh. Mesh devices were implanted in a partial thickness abdominal wall defect in the rat. Following explantation, the mesh materials and associated tissue were immunolabeled for cell surface markers associated with M1 and M2 macrophage phenotypes at time points ranging from 3 to 35 days. All animal experiments were conducted in accordance to University of Pittsburgh Institutional Animal Care and Use Committee (IACUC) regulations and guidelines.

2.2. ECM preparation and mesh coating

Dermal ECM (D-ECM) was prepared by decellularization of porcine skin as previously described [15, 25]. The epidermis and subcutaneous tissue were mechanically removed to isolate the dermal layer (thickness approximately 1.5 mm), which was enzymatically and chemically decellularized. In brief, dermis was treated with 0.25% Trypsin (Sigma) for 6 hours, 70% ethanol for 10 hours, hydrogen peroxide for 15 min, 1% Triton X-100 in 0.26% EDTA/0.69% Tris-base for 6 hours followed by an additional 16 hours in fresh solution, and 0.1% peracetic acid/4% ethanol for 2 hours. All steps were performed at room temperature with agitation by an orbital shaker (300RPM) and extensive rinsing (3×15min washes with deionized water) after each step.

Urinary bladder matrix ECM was prepared from porcine urinary bladders via mechanical isolation of the basement membrane and subjacent *tunica propria* layers as previously described [14, 25]. The tissue was rinsed in deionized water and decellularized with 0.1% PAA/4% ethanol (v/v) 2 hours associated with agitation by an orbital shaker (300 RPM). The resulting UBM-ECM was rinsed extensively with PBS and deionized water.

Both D-ECM and UBM-ECM scaffolds were frozen, lyophilized, and comminuted into a particulate using a Wiley Mill passed through a 40 mesh screen [25, 26]. ECM powder was enzymatically digested and solubilized at an ECM concentration of 10 mg ECM (dry wt)/ml with 1 mg/ml pepsin in 0.01 M HCl. ECM pre-gel was prepared by neutralizing the partially digested ECM with 1/9 digest volume of 10X PBS, 1/10 the digest volume of 0.1 M NaOH, and dilution with 1X PBS to a final ECM concentration of 8 mg ECM (dry wt.)/ml. Heavy-weight polypropylene mesh (BARD Mesh, C.R. BARD-Davol, Providence, RI) coupons (1 cm × 1 cm) were embedded within molds (1.2 cm × 1.2 cm) containing D-ECM or UBM-ECM pre-gel solutions and placed in a non-humidified incubator at 37°C to initiate gelation. ECM hydrogels formed around the polypropylene mesh fibers and either remained in a

hydrated form (D-ECM wet and UBM-ECM wet) or were further dried in a non-humidified incubator at 37°C for 24 hours (D-ECM dry and UBM-ECM dry) [16]. All devices were sterilized prior to implantation with 2Mrad gamma irradiation at room temperature.

Mesh coating structure was evaluated macroscopically and by scanning electron microscopy. Mesh devices were fixed with 2.5% glutaraldehyde for 24 hours and washed with PBS. Devices were then dehydrated with a graded series of ethanol (30%, 50%, 70%, 90%) for 2 hours each and three overnight washes in 100% ethanol with gentle agitation. Mesh devices were then critically point dried using carbon dioxide as the transitional drying medium. Samples were sputter coated with a 3.5 nm gold palladium alloy and imaged using 10keV accelerating voltage. Images were acquired of both the mesh surfaces and cross sections at low (50X) and high (500X) magnifications.

2.3. Mesh implantation in rodent model

Uncoated and ECM coated mesh devices were implanted in an established abdominal wall injury model in the rat [25, 27]. Female rats (250-300g, Sprague-Dawley, Charles River Laboratories Inc., Wilmington, MA) were anesthetized with 1.5-3% isofluorane. Bilateral paramedian skin incisions were made to provide access to the muscular abdominal wall, and partial thickness skeletal muscle defects were created by excision of 1 cm × 1 cm segments of the external and internal oblique muscles while leaving the underlying *transversalis fascia* intact. Mesh device groups were inlaid within the muscle defect and affixed to the abdominal wall with polypropylene sutures (Prolene) at each corner. Animals were allowed to recover and ambulate normally until sacrifice with mesh explantation at 3, 7, 14, or 35 days (n = 5 per device at each time point).

2.4. Spatiotemporal analysis of macrophage phenotype

Explanted mesh with surrounding abdominal wall tissue was fixed with 10% neutral buffered formalin for at least 24 hours, embedded in paraffin, and sectioned (5 μm). Immnofluorescent labeling was performed to characterize macrophage phenotype in response to ECM coated and uncoated polypropylene mesh test articles. Slides were deparaffinized followed by antigen retrieval in heated citrate buffer for 20 minutes (10 mM citrate, pH 6.0 at 95-100°C). Non-specific antibody binding was prevented via incubation for 1 hour at room temperature with a blocking solution consisting of 2% normal horse serum (Hyclone), 1% bovine serum albumin (Sigma), 0.1% Triton X-100 (Sigma), and 0.1% Tween-20 (Sigma) in PBS. Sections were decanted and incubated with primary antibodies diluted 1:150 in blocking solution overnight at 4°C. Primary antibodies against the pan-macrophage marker CD68 (mouse anti-rat CD68, clone ED1, Abd Serotec), the M1 macrophage marker CD86 (rabbit anti-human CD86, clone EP1158Y, Abcam), and the M2 macrophage marker CD206 (goat anti-human CD206, polyclonal, Santa Cruz) were used. Sections were washed and incubated with the following fluorescently conjugated secondary antibodies diluted in blocking solution for 1 hour at room temperature: donkey anti-mouse Alexa Fluor-594 (1:200 dilution, Invitrogen), donkey anti-rabbit PerCP-Cy5.5 (1:300 dilution, Santa Cruz), and donkey anti-goat Alex Fluor-488 (1:200 dilution, Invitrogen). Nuclei were labeled with DAPI and slides coverslipped with fluorescent mounting medium (Dako). Multispectral epifluorescent images were acquired (Nuance) and spectrally unmixed

to remove background autofluorescence. A total of 6 high magnification images (400X) distributed across 2 locations within the mesh device were acquired (**Figure 1A, boxes)**. Representative fields of view were centered at both the mesh fiber pore interface adjacent to single fibers (**Figure 1B**) and centered within mesh knot structures (**Figure 1C**). The total number of cells co-expressing CD68 and either CD86 or CD206 was automatically quantified for each image using CellProfiler software (http://www.cellprofiler.org, [28]). Macrophages were defined as CD68 positive colocalized with nuclei. M1 and M2 cells were defined as macrophages coexpressing CD86 or CD206, respectively. A subpopulation of cells co-expressed both M1 and M2 markers and were subsequently denoted as “co-labeled”. Macrophage spatial distribution relative to mesh fibers was characterized by defining concentric rings around mesh fibers that were evenly spaced at 33 μm intervals as shown in **Figure 1**. A total of 5 ring areas were defined around single fibers and 3 rings within fiber knots. Cells on the border of 2 rings were counted towards the inner ring and any overlapping ring areas between knots were counted only once. The total number of macrophages in each phenotypic state and the ratio of M2:M1 macrophages were determined for each device/time point/spatial location. The M2:M1 ratio was calculated as the (# of M2 macrophages + 1) / (# M1 macrophages + 1) to accommodate conditions in which there were no M1 and/or M2 macrophages present within the region of interest.

2.5. Histomorphometric quantification

Histologic remodeling was evaluated from Masson’s Trichrome stained sections as previously described [16]. High magnification (400X) images were acquired using the same strategy described above: adjacent to single fibers and within fiber knots. The total number of multinucleate foreign body giant cells and blood vessels was counted by blinded observers for each image. Multinucleate foreign body giant cells were defined as any large cell at the mesh fiber surface containing 2 or more nuclei. Blood vessels were functionally defined as structures possessing a lumen with red blood cells within.

2.6. Statistical analysis

The total number of macrophages, macrophage ratio, and histomorphometric data are presented as the mean ± the standard error of the mean. Statistical analysis was performed using a one-way ANOVA evaluating each spatial location (e.g. ring 1 or ring 2) for each variable (M1, M2, etc) within each time point using SPSS software. A post-hoc Tukey test was conducted with a p-value < 0.05 considered statistically significant. Data normality was determined using the Kolmgorov-Smirnov test, and natural logarithm transformation applied when normality was violated.

3. Results

3.1. ECM preparation and mesh coating

D-ECM and UBM-ECM were prepared from porcine dermis and urinary bladder tissue, respectively, and processed into a hydrogel form. Polypropylene mesh coupons (**Figure 2A**) were embedded within ECM hydrogels (**Figure 2B-E**). Both dried and wet ECM coatings fully covered the mesh fiber surface and filled the pores between mesh fibers, as well as within the interstices between mesh fiber knots as shown by macroscopic observation and

SEM (**Figure 2G-J, inset**). Ultrastructural examination showed that the smooth surface of polypropylene mesh fibers (**Figure 2F**) was covered with ECM hydrogels that imparted distinct structural characteristics depending upon the type of coating. Both UBM-ECM and D-ECM wet hydrogel coatings (**Figure 2G,-J**) had a randomly oriented fibrillar structure, and the D-ECM fibril network was more dense than UBM-ECM. Drying the ECM hydrogel coating induced structural changes to both UBM-ECM and D-ECM hydrogel coatings (**Figure 2H, J**). The dried hydrogel coatings appeared as a textured surface of randomly oriented raised patterns and indentations reminiscent of collapsed ECM fibrils.

SEM cross sections confirmed the presence of both wet and dried ECM hydrogel coating throughout the mesh pores and within mesh fiber knots. The wet ECM hydrogel coatings (**Figure 2L,N, inset**) had fibrillar structural characteristics (**Figure 2L,N**) that were similar to the surface images. UBM-ECM and D-ECM dried hydrogel coatings were very thin compared to the wet hydrogels (**Figure 2M,O inset**) and tightly conformed to the mesh fiber topography. High magnification ross sections of dried ECM coatings showed lamellar sheets with occasional fibrils crossing between layers (**Figure 2M,O**).

3.2. Spatiotemporal analysis of macrophage phenotype

Macrophage phenotype was evaluated via the coexpression of the pan-macrophage cell surface marker CD68 with the M1 marker CD86 and/or the M2 marker CD206. Macrophage phenotypic expression in response to an uncoated polypropylene mesh was similar in areas both adjacent to single fibers (**Figure 3A**) and within fiber knots (**Figure 3B**) and characterized by a dominant M1 response. The number of M1 macrophages was greatest in ring 1, which was the area in closest proximity to the mesh fiber, and decreased with increased distance from the mesh fiber approaching background levels by ring 3 in areas adjacent to single fibers. The number of M2 and M1+M2 co-labeled macrophages remained at low background levels at all time points. The initial day 3 M1 response within ring 1 markedly increased by day 7, and remained approximately constant at the 14 and 35 day time points. This pattern of macrophage distribution was observed for both individual mesh fiber and at fiber knot locations.

Each ECM coating type reduced the total number of macrophages present directly adjacent to single fibers compared to an uncoated mesh at the evaluated time points (**Figure 4**). Similar to the uncoated mesh, the M1 accumulation was greatest in ring 1 and rapidly decreased with distance. The number of M1 macrophages around ECM coated mesh was lowest at the day 3 time point, and were not different from the uncoated mesh. Only the D-ECM dry coating affected the M1 response within ring 1 at day 7, though by day 14, each coating had reduced the M1 response, except for the UBM-ECM dry coating. The effect of the ECM coating was most pronounced by the 35 day time point, where M1 macrophage accumulation was attenuated at all distances (rings 1-5). Few differences in the number of M1 cells were observed between different ECM coating types, and none of the coating types consistently affected the number of M2 cells at any time point or distance. The effect of each ECM coating was also evaluated by calculating the ratio of M2 to M1 macrophages (**Figure 5**). All ECM coatings except for the UBM-ECM dry increased the M2:M1 ratio within rings 1 and 2 adjacent to individual fibers by 14 days, but not at earlier time points. An increased

M2:M1 ratio continued primarily for both the UBM-ECM and D-ECM wet hydrogel coatings at 35 days.

The ECM coatings had a similar effect within fiber knots; a location in which ECM coatings reduced the M1 response compared to an uncoated mesh at day 7, 14, and 35 time points (**Figure 6**). Though the number of M1 cells diminished with distance from the mesh fiber, the reduction in M1 cells for all ECM coatings typically persisted through rings 1-3. All ECM coatings significantly decreased the number of M1 cells in rings 2-3 by 7 days and in most rings at day 14. All coatings except for UBM-ECM dry reduced the M1 response in rings 1-2 at day 35 with no differences by ring 3. There were no differences in the number of M1 cells between different ECM coating types at any time point except at the 3 day time point where the number of M1 macrophages was greater for the UBM-ECM wet hydrogel coating. There were fewer M2 macrophages compared to M1 for all test articles, with only minor increases in number of M2 cell resulting from ECM coating. The ratio of M2:M1 macrophages within the knots of uncoated polypropylene mesh was increased by ECM coatings following the 3 day time point (**Figure 7**). Only the UBM-ECM and D-ECM wet hydrogel coatings showed an increased M2:M1 ratio at the 7 day time point, and the M2:M1 ratio for all ECM coatings except for the dried UBM-ECM was increased at all distances at the 14 day time point. The increased M2:M1 ratio was observed for all ECM coatings at the 35 day time point at ring 2, and for all coatings except for dried UBM-ECM within ring 1. There were no differences in the M2:M1 ratio of different ECM coatings at any time point, except between UBM-ECM dry and wet coatings at day 3.

3.3. Histomorphometric quantification

Histologic remodeling outcomes for uncoated and ECM coated mesh were determined from Masson's Trichrome stained images, and the number of foreign body giant cells and blood vessels were counted adjacent to single mesh fibers (**Figure 8A**) and within mesh fiber knots (**Figure 8J**). Foreign body giant cells adjacent to single fibers in uncoated mesh began to form by the 7 day time point, peaked by 14 days, and had declined by 35 days. Each ECM coating showed a similar reduction in the number of giant cells at the 14 day time point, though there were no differences from uncoated mesh by 35 days. The number of blood vessels adjacent to single mesh fibers increased between increased between 3 and 14 day time points for all devices. There were fewer vessels around D-ECM coated mesh at the 7 day time point compared to uncoated and UBM coated mesh, but no differences at later time points.

Foreign body giant cell formation between mesh fiber knots was apparent by 7 days and was greatest at the 14 and 35 day time points for all devices. A greater number of foreign body giant cells was observed between uncoated mesh fiber knots compared to ECM coated mesh at 7, 14, and 35 day time points. The number of blood vessels within knots increased between 3 and 14 days. Except for a reduction in blood vessel formation at the 3 day time point, ECM coatings did not result in a There were no distinguishable differences in blood vessel formation within knots as the result of any ECM coating.

4. Discussion

The present study investigated the effect of ECM hydrogel coatings derived from two separate source tissues, porcine urinary bladder and dermis, upon macrophage phenotype in response to a knitted heavy-weight polypropylene mesh. Both tissue sources of ECM coating reduced the prevalence of pro-inflammatory M1 polarized macrophages and foreign body giant cells adjacent to mesh fibers when applied in hydrated or dried forms. The immunomodulatory effect of ECM coating was apparent around both single mesh fibers and within mesh fiber knots.

Ventral hernia repair commonly utilizes non-degradable, synthetic polymers such as polypropylene to reinforce the repair of weakened or ruptured abdominal wall tissue. Such synthetic materials have properties that are desirable for hernia repair such as high mechanical strength and incorporation of the mesh into the surrounding host tissue, resulting in notable reductions in hernia recurrence compared to primary repair [8, 29]. A consequence of implanting a non-degradable material however, is a robust foreign body reaction with associated scar tissue formation [3]. The reported sequelae of dense scar formation surrounding and within the mesh material include contracture, loss of compliance, adhesions, and/or fistula formation, potentially necessitating surgical intervention [9, 10].

Alternatives to non-degradable/slowly degrading synthetic materials are under investigation to minimize the downstream consequences of the foreign body reaction. ECM devices prepared from decellularized xenogeneic or allogeneic tissues have been used to promote more favorable remodeling outcomes for hernia repair [11, 30, 31]. The ECM is a complex microenvironment comprised of collagen types, glycosaminoglycans, growth factors, and proteoglycans that are maintained during the cell removal process, and supports site appropriate tissue remodeling rather than scar formation [11, 12]. Several mechanisms and determinants have been implicated in the ECM remodeling response including the recruitment of endogenous stem and progenitor cells, growth factor sequestration [15, 32], release of bioactive ECM fragments during the degradation process [33, 34], and modulation of the innate immune response, namely macrophage phenotype [19]. ECM hydrogels composed of *in vitro* degradation products have been derived from the ECM of many source tissues such as dermis, cardiac, urinary bladder, and central nervous system and they exhibit many of the positive remodeling properties that have also been found in the intact scaffold [25, 35, 36]. A recent study described the application of a dried dermal ECM hydrogel to a synthetic polypropylene mesh, and showed that the coating imparted several favorable effects in rodent abdominal wall defect model [16]. The D-ECM dry coating altered the default host response to a polypropylene mesh, including reducing the number of foreign body giant cells and density of deposited collagen without compromising mechanical strength or tissue incorporation. Although it was shown that an ECM hydrogel mitigated the foreign body reaction and subsequent tissue remodeling, the mechanisms by which these events occurred were not investigated.

Macrophage dynamics at the biomaterial surface have been well characterized and associated with the foreign body reaction [4, 7]. Within 3-5 days of implantation, macrophages accumulate at the implant site, and if the material is not able to be

phagocytosed, macrophage presence will persist, and eventually culminates in macrophage fusion into multinucleate giant cells that surround the foreign body. The macrophage response to a foreign body has been described from a histopathologic perspective, though it has been shown in recent years that macrophages are a heterogeneous population of cells that are polarized by microenvironmental cues toward distinct functional phenotypes: the pro-inflammatory M1 phenotype or an anti-inflammatory M2 phenotype (reviewed in [22, 23]). The M1 phenotype is classically associated with pro-inflammatory host defense functions such as antimicrobial activity and phagocytosis, and the alternatively activated M2 phenotype, in contrast, is involved with resolution of inflammation and wound healing [22, 23]. Indeed, several studies have explored the M1/M2 macrophage paradigm in response to implanted ECM scaffolds [18-20, 24]. These studies have shown that ECM scaffolds are rapidly infiltrated by M1 and M2 macrophages, though with a greater proportion of M2 macrophages than is seen with non-degradable materials. The differential polarization state of macrophages in response to ECM biomaterials has been shown to be an important determinant of remodeling outcome, though a detailed analysis of the macrophage polarization response to polyproplylene mesh has not been conducted.

The present study found a robust accumulation of pro-inflammatory M1 macrophages at the mesh-tissue interface as early as 7 days following implantation, which persisted until the 35 day time point. Spatially, M1 accumulation was greatest directly adjacent to the mesh fibers, and rapidly diminished with distance to background levels by approximately 100 μm from the implant surface, suggesting a localized pro-inflammatory response to polypropylene. Though the M1 response was confined within close proximity to the mesh, pro-inflammatory cytokine release may still affect remodeling outcomes distal to the mesh. Conversely, there were relatively few anti-inflammatory M2 macrophages, reinforcing the assertion that a non-degradable polypropylene mesh induces a pro-inflammatory environment.

ECM coatings affected the macrophage response to polypropylene primarily by reducing the pro-inflammatory M1 response at the implant-tissue interface, while inducing a minimal effect upon the M2 response. The M1 reduction, and resultant increase in M2:M1 ratio, caused by the ECM coatings was greatest within the area nearest the polypropylene mesh, where the default M1 response was most intense. All coating types showed a decrease in M1 cells, though the wet hydrogel coatings from both UBM-ECM and D-ECM sources more consistently resulted in these reductions. The wet hydrogel coatings were composed of a dense fibrillar network and were thicker than the compact dry coating as shown by SEM. These structural differences may affect macrophage phenotype since they have been shown to respond to mechanical and structural cues in addition to specific cytokines and molecular signals [37-40]. These results suggest that the coating structure may influence the response, though significant differences between different coating types were not consistently observed.

Synthetic mesh devices, including the polypropylene mesh used in the present study, are frequently composed of many individual fibers knitted together into one cohesive construct. This configuration places several fibers in close proximity to each other in fiber knots, and the space within these knots is influenced by a greater amount of polypropylene than around

single fibers. Both wet and dry UBM-ECM and D-ECM coatings filled these spaces, and reduced the pro-inflammatory M1 response within these regions, though the UBM-ECM dry coating less consistently produced this effect. These findings show that the ECM coatings can maintain immune modulating properties in the presence of highly pro-inflammatory stimuli such as a high density and surface area of foreign material.

There are several potential limitations to the present study. M1 and M2 macrophages were identified by single surface markers, though macrophage polarization is most appropriately considered as a spectrum and involves numerous signaling and effector proteins. The M2/M1 expression profile may differ greatly depending on the location along this spectrum, which is further complicated by the ability of macrophages to switch phenotypes depending on their current signaling environment [23]. A small population of macrophages in this study co-expressed M1 and M2 associated markers, which may indicate a transition state between M1 and M2 phenotypes. The generalization of the M2 phenotype may also be an oversimplification. M2 macrophage polarization during wound healing can be subdivided into M2a, M2b, and M2c subtypes, each of which has distinct immunoregulatory functions [22]. CD206 is generally associated as a marker of the M2a phenotype, but markers of other M2 subtypes, such as the M2c marker CD163, and their potential roles in tissue remodeling were not considered in the present study. Additional surface markers and/or secreted products may be analyzed using this spatiotemporal framework to specifically categorize the response and understand the signaling pathways involved.

5. Conclusions

Hydrogel coatings composed of dermal or urinary bladder ECM are able to modulate the default innate immune response to heavy-weight polypropylene mesh *in vivo*. ECM primarily attenuated the M1 response and foreign body giant cell formation around mesh devices in a specific spatial and temporal pattern, which was not dependent upon the tissue source or structure of the ECM coating. Improved remodeling response previously reported for an ECM coated polypropylene mesh compared to an uncoated mesh may be the result of macrophage polarization and consequent signaling during host remodeling. ECM hydrogel coatings may therefore be viable modification method to alleviate the chronic inflammatory response to non-degradable implanted medical devices.

6. Acknowledgements

Matthew Wolf was partially supported by the NIH-NHLBI training grant (T32-HL76124-6) entitled “Cardiovascular Bioengineering Training Program” through the University of Pittsburgh Department of Bioengineering, and Bryan Brown was partially supported by the NIH K12 clinical scientist development program (HD043441). The authors would like to acknowledge Deanna Rhoads of the McGowan histology center for histologic sample preparation, and the University of Pittsburgh Center for Biologic Imaging (CBI) for access to SEM imaging facilities.

References

[1]. Hollinsky C, Sandberg S, Koch T, Seidler S. Biomechanical properties of lightweight versus heavyweight meshes for laparoscopic inguinal hernia repair and their impact on recurrence rates. Surg Endosc. 2008; 22(12):2679–85. [PubMed: 18443869]

[2]. Feola A, Barone W, Moalli P, Abramowitch S. Characterizing the ex vivo textile and structural properties of synthetic prolapse mesh products. Int Urogynecol J. 2013; 24(4):559–64. [PubMed: 22885725]

[3]. Klosterhalfen B, Junge K, Klinge U. The lightweight and large porous mesh concept for hernia repair. Expert Rev Med Devices. 2005; 2(1):103–17. [PubMed: 16293033]

[4]. Anderson JM, Rodriguez A, Chang DT. Foreign body reaction to biomaterials. Semin Immunol. 2008; 20(2):86–100. [PubMed: 18162407]

[5]. Klinge U, Klosterhalfen B, Muller M, Schumpelick V. Foreign body reaction to meshes used for the repair of abdominal wall hernias. Eur J Surg. 1999; 165(7):665–73. [PubMed: 10452261]

[6]. Luttikhuizen DT, Harmsen MC, Van Luyn MJ. Cellular and molecular dynamics in the foreign body reaction. Tissue Eng. 2006; 12(7):1955–70. [PubMed: 16889525]

[7]. McNally AK, Anderson JM. Macrophage fusion and multinucleated giant cells of inflammation. Adv Exp Med Biol. 2011; 713:97–111. [PubMed: 21432016]

[8]. Cobb WS, Kercher KW, Heniford BT. The argument for lightweight polypropylene mesh in hernia repair. Surg Innov. 2005; 12(1):63–9. [PubMed: 15846448]

[9]. Leber GE, Garb JL, Alexander AI, Reed WP. Long-term complications associated with prosthetic repair of incisional hernias. Arch Surg. 1998; 133(4):378–82. [PubMed: 9565117]

[10]. Costello CR, Bachman SL, Ramshaw BJ, Grant SA. Materials characterization of explanted polypropylene hernia meshes. J Biomed Mater Res B Appl Biomater. 2007; 83(1):44–9. [PubMed: 17285608]

[11]. Badylak SF. The extracellular matrix as a biologic scaffold material. Biomaterials. 2007; 28(25): 3587–93. [PubMed: 17524477]

[12]. Badylak SF, Weiss DJ, Caplan A, Macchiarini P. Engineered whole organs and complex tissues. Lancet. 2012; 379(9819):943–52. [PubMed: 22405797]

[13]. Crapo PM, Gilbert TW, Badylak SF. An overview of tissue and whole organ decellularization processes. Biomaterials. 2011; 32(12):3233–43. [PubMed: 21296410]

[14]. Freytes DO, Stoner RM, Badylak SF. Uniaxial and biaxial properties of terminally sterilized porcine urinary bladder matrix scaffolds. J Biomed Mater Res B Appl Biomater. 2008; 84(2): 408–14. [PubMed: 17618508]

[15]. Reing JE, Brown BN, Daly KA, Freund JM, Gilbert TW, Hsiong SX, et al. The effects of processing methods upon mechanical and biologic properties of porcine dermal extracellular matrix scaffolds. Biomaterials. 2010; 31(33):8626–33. [PubMed: 20728934]

[16]. Wolf MT, Carruthers CA, Dearth CL, Crapo PM, Huber A, Burnsed OA, et al. Polypropylene surgical mesh coated with extracellular matrix mitigates the host foreign body response. J Biomed Mater Res A. 2014; 102(1):234–46.

[17]. Allman AJ, McPherson TB, Badylak SF, Merrill LC, Kallakury B, Sheehan C, et al. Xenogeneic extracellular matrix grafts elicit a TH2-restricted immune response. Transplantation. 2001; 71(11):1631–40. [PubMed: 11435976]

[18]. Valentin JE, Stewart-Akers AM, Gilbert TW, Badylak SF. Macrophage participation in the degradation and remodeling of extracellular matrix scaffolds. Tissue Eng Part A. 2009; 15(7): 1687–94. [PubMed: 19125644]

[19]. Badylak SF, Valentin JE, Ravindra AK, McCabe GP, Stewart-Akers AM. Macrophage phenotype as a determinant of biologic scaffold remodeling. Tissue Eng Part A. 2008; 14(11): 1835–42. [PubMed: 18950271]

[20]. Brown BN, Londono R, Tottey S, Zhang L, Kukla KA, Wolf MT, et al. Macrophage phenotype as a predictor of constructive remodeling following the implantation of biologically derived surgical mesh materials. Acta Biomater. 2012; 8(3):978–87. [PubMed: 22166681]

[21]. Fishman JM, Lowdell MW, Urbani L, Ansari T, Burns AJ, Turmaine M, et al. Immunomodulatory effect of a decellularized skeletal muscle scaffold in a discordant xenotransplantation model. Proc Natl Acad Sci U S A. 2013; 110(35):14360–5. [PubMed: 23940349]

[22]. Mantovani A, Sica A, Sozzani S, Allavena P, Vecchi A, Locati M. The chemokine system in diverse forms of macrophage activation and polarization. Trends Immunol. 2004; 25(12):677–86. [PubMed: 15530839]

[23]. Mantovani A, Biswas SK, Galdiero MR, Sica A, Locati M. Macrophage plasticity and polarization in tissue repair and remodelling. J Pathol. 2013; 229(2):176–85. [PubMed: 23096265]

[24]. Brown BN, Valentin JE, Stewart-Akers AM, McCabe GP, Badylak SF. Macrophage phenotype and remodeling outcomes in response to biologic scaffolds with and without a cellular component. Biomaterials. 2009; 30(8):1482–91. [PubMed: 19121538]

[25]. Wolf MT, Daly KA, Brennan-Pierce EP, Johnson SA, Carruthers CA, D'Amore A, et al. A hydrogel derived from decellularized dermal extracellular matrix. Biomaterials. 2012; 33(29): 7028–38. [PubMed: 22789723]

[26]. Freytes DO, Martin J, Velankar SS, Lee AS, Badylak SF. Preparation and rheological characterization of a gel form of the porcine urinary bladder matrix. Biomaterials. 2008; 29(11): 1630–7. [PubMed: 18201760]

[27]. Valentin JE, Turner NJ, Gilbert TW, Badylak SF. Functional skeletal muscle formation with a biologic scaffold. Biomaterials. 2010; 31(29):7475–84. [PubMed: 20638716]

[28]. Carpenter AE, Jones TR, Lamprecht MR, Clarke C, Kang IH, Friman O, et al. CellProfiler: image analysis software for identifying and quantifying cell phenotypes. Genome Biol. 2006; 7(10):R100. [PubMed: 17076895]

[29]. George CD, Ellis H. The results of incisional hernia repair: a twelve year review. Ann R Coll Surg Engl. 1986; 68(4):185–7. [PubMed: 3789602]

[30]. Ansaloni L, Catena F, Coccolini F, Gazzotti F, D'Alessandro L, Pinna AD. Inguinal hernia repair with porcine small intestine submucosa: 3-year follow-up results of a randomized controlled trial of Lichtenstein's repair with polypropylene mesh versus Surgisis Inguinal Hernia Matrix. Am J Surg. 2009; 198(3):303–12. [PubMed: 19285658]

[31]. Hiles M, Record Ritchie RD, Altizer AM. Are biologic grafts effective for hernia repair?: a systematic review of the literature. Surg Innov. 2009; 16(1):26–37. [PubMed: 19223383]

[32]. Voytik-Harbin SL, Brightman AO, Kraine MR, Waisner B, Badylak SF. Identification of extractable growth factors from small intestinal submucosa. J Cell Biochem. 1997; 67(4):478–91. [PubMed: 9383707]

[33]. Reing JE, Zhang L, Myers-Irvin J, Cordero KE, Freytes DO, Heber-Katz E, et al. Degradation products of extracellular matrix affect cell migration and proliferation. Tissue Eng Part A. 2009; 15(3):605–14. [PubMed: 18652541]

[34]. Beattie AJ, Gilbert TW, Guyot JP, Yates AJ, Badylak SF. Chemoattraction of progenitor cells by remodeling extracellular matrix scaffolds. Tissue Eng Part A. 2009; 15(5):1119–25. [PubMed: 18837648]

[35]. DeQuach JA, Yuan SH, Goldstein LS, Christman KL. Decellularized porcine brain matrix for cell culture and tissue engineering scaffolds. Tissue Eng Part A. 2011; 17(21-22):2583–92. [PubMed: 21883047]

[36]. Seif-Naraghi SB, Singelyn JM, Salvatore MA, Osborn KG, Wang JJ, Sampat U, et al. Safety and efficacy of an injectable extracellular matrix hydrogel for treating myocardial infarction. Sci Transl Med. 2013; 5(173):173ra25.

[37]. Sussman, EM.; Halpin, MC.; Muster, J.; Moon, RT.; Ratner, BD. Porous Implants Modulate Healing and Induce Shifts in Local Macrophage Polarization in the Foreign Body Reaction. Ann Biomed Eng. 2013. Available from URL: http://www.ncbi.nlm.nih.gov/pubmed/24248559 (DOI: 10.1007/s10439-013-0933-0)

[38]. McWhorter FY, Wang T, Nguyen P, Chung T, Liu WF. Modulation of macrophage phenotype by cell shape. Proc Natl Acad Sci U S A. 2013; 110(43):17253–8. [PubMed: 24101477]

[39]. Blakney AK, Swartzlander MD, Bryant SJ. The effects of substrate stiffness on the in vitro activation of macrophages and in vivo host response to poly(ethylene glycol)-based hydrogels. J Biomed Mater Res A. 2012; 100(6):1375–86. [PubMed: 22407522]

[40]. Bernatchez SF, Parks PJ, Gibbons DF. Interaction of macrophages with fibrous materials in vitro. Biomaterials. 1996; 17(21):2077–86. [PubMed: 8902241]

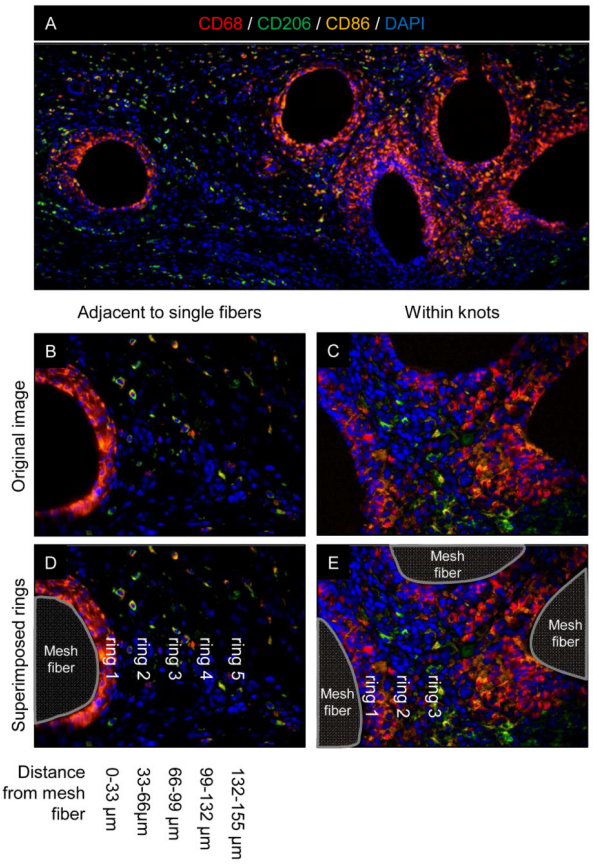

Figure 1.

Histologic mesh imaging and spatial quantification of polarized macrophages. Representative low magnification (100X) immunofluorescent image of an uncoated polypropylene mesh (A) with white boxes indicating the regions of interest for high magnification image acquisition (400X) for macrophage quantification . Images were acquired at the edge of single mesh fibers (B) and within mesh fiber knots (C). The spatial distribution of polarized macrophages relative to the tissue-mesh fiber interface was quantified within the areas of concentric rings (dotted lines) evenly spaced around mesh fibers (D,E). Each ring represents an increased radius of 33 µm from the mesh fiber. Macrophage phenotype was identified via surface markers: CD68+ pan-macrophage (red), CD86+ M1 macrophage (orange), and CD206+ M2 macrophage (green) colocalized with DAPI stained nuclei (blue). Scale bars represent 100 µm.

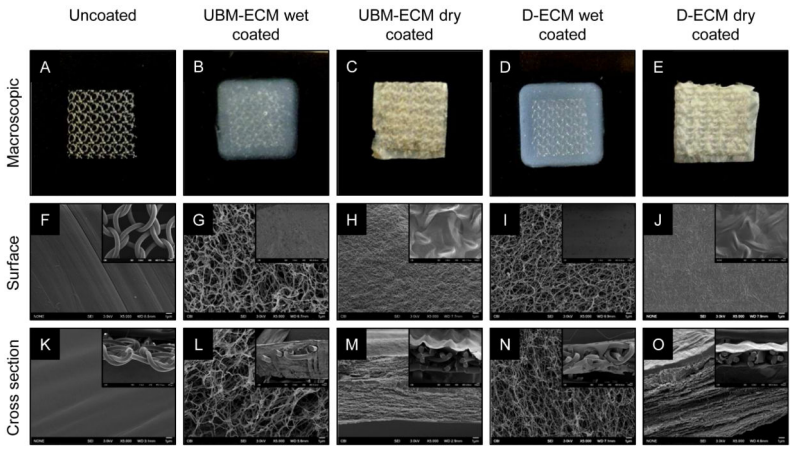

Figure 2.

ECM coating coverage and structure. Representative macroscopic images of uncoated polypropylene mesh (A), UBM-ECM wet hydrogel coated mesh (B), UBM-ECM dried hydrogel coated mesh (C), D-ECM wet hydrogel coated mesh (D), and dried D-ECM hydrogel coated mesh (E). Scale bar represents 1 cm. Scanning electron micrographs of the surfaces and cross sections of uncoated and wet/dried ECM coated hydrogel coated mesh. High magnification images of mesh structure (5,000X) are provided with low magnification images of coating coverage (50X, inset).

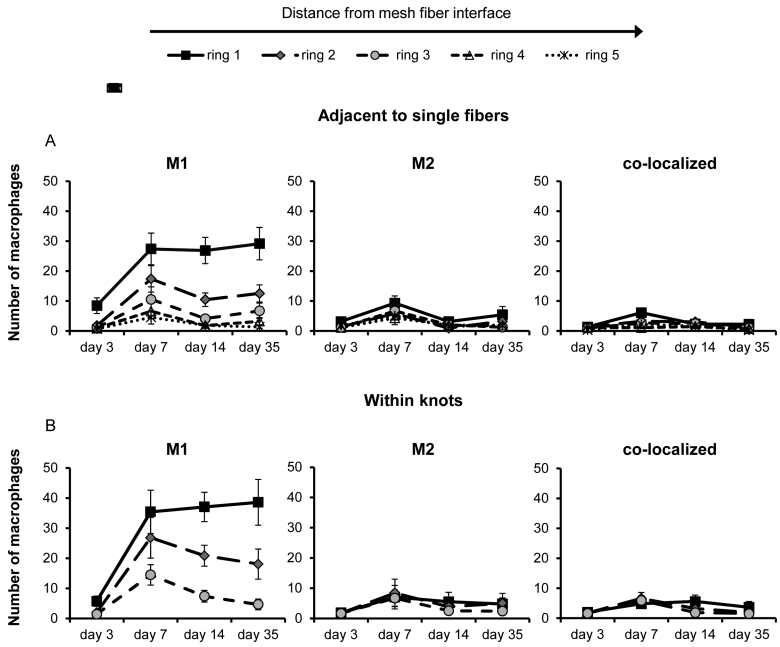

Figure 3.

Spatiotemporal macrophage response to uncoated polypropylene mesh. The number of M1 (CD86+/CD68+), M2 (CD206+/CD68+), an co-localized (CD86+/CD206+/CD68+) macrophages adjacent to single mesh fibers (A) and within knots (B) were quantified with respect to distance from the tissue-mesh fiber interface. Each ring (1-5) represents increasing distance from the mesh fiber surface after 3, 7, 14, and 35 days post implantation.

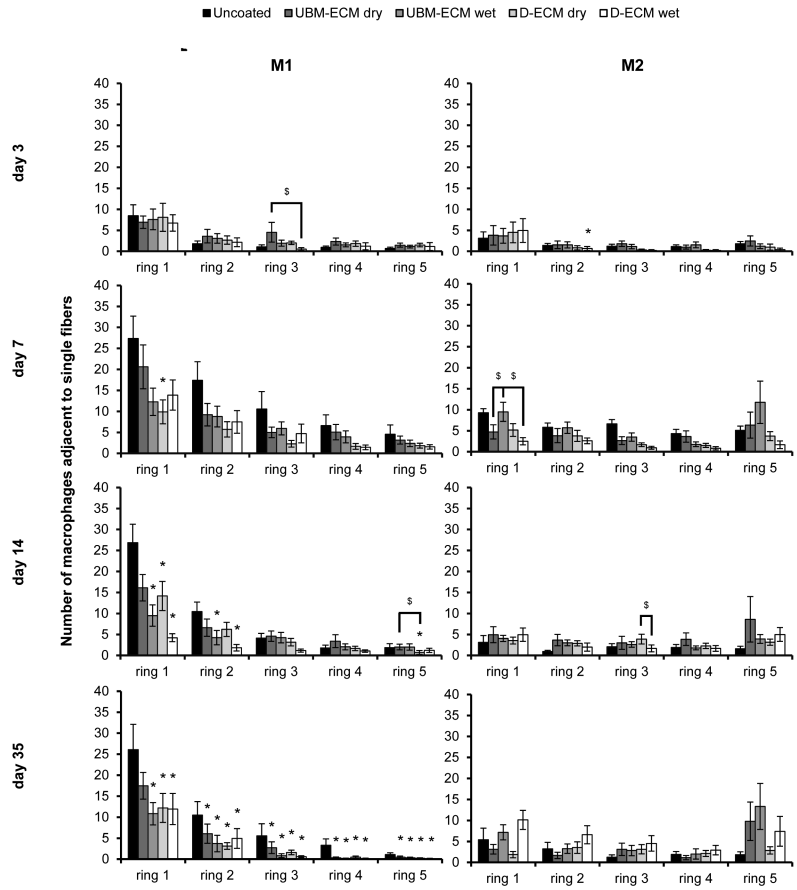

Figure 4.

Macrophage polarization adjacent to single mesh fibers in uncoated and ECM hydrogel coated mesh. The number of M1 (CD86+/CD68+) and M2 (CD206+/CD68+) macrophages in response to uncoated, UBM-ECM dry coated, UBM-ECM wet coated, D-ECM dry coated, and D-ECM wet coated polypropylene mesh were quantified from high magnification images of implanted mesh adjacent to single fibers. Total M1 and M2 macrophages were counted at each increasing distance interval from the mesh fiber surface (ring 1-5) at 3, 7, 14, and 35 day time points. Statistical significant differences were determined with ANOVA ($p < 0.05$) and denoted with (*) as different from uncoated mesh, or ($) as different between ECM coating groups.

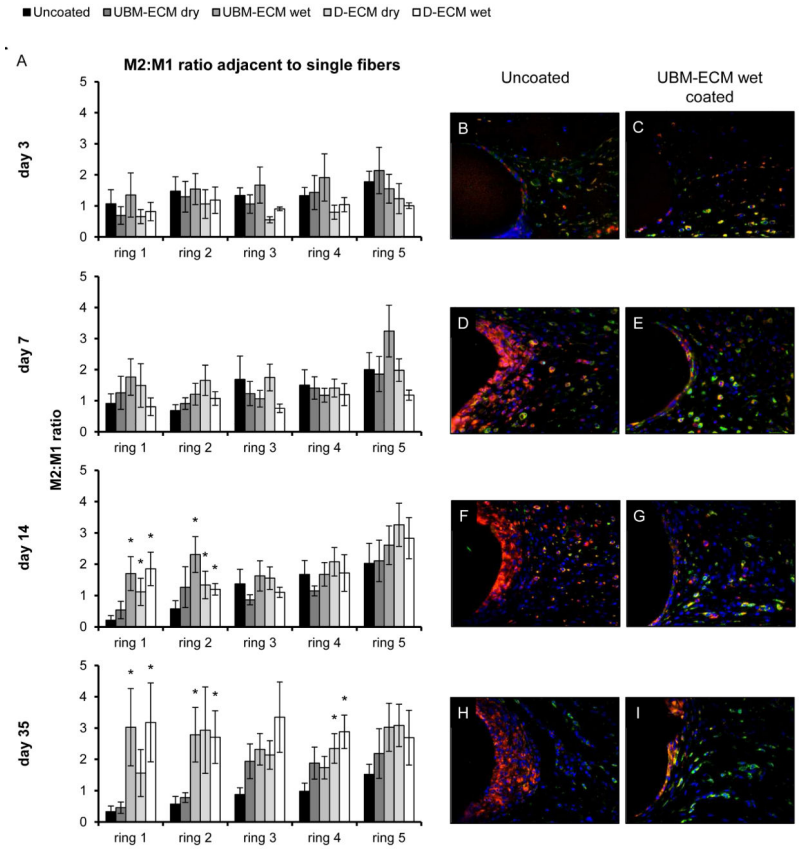

Figure 5.

M2:M1 polarized macrophage ratio adjacent to single mesh fibers. The ratio of M2 to M1macrophages in response to uncoated, UBM-ECM dry coated, coated UBM-ECM wet coated, D-ECM dry coated, and D-ECM wet coated polypropylene mesh was determined with distance (ring 1-5) from the mesh fiber surface at 3, 7, 14, and 35 days post implantation (A). Representative images of uncoated polypropylene mesh (B,D,F,H) and UBM-ECM wet coated mesh (C,E,G,I) are shown at each time point. Statistical significant differences were determined with ANOVA ($p < 0.05$) and denoted with (*) as different from uncoated mesh, or ($) as different between ECM coating groups. Scale bar represents100 μm.

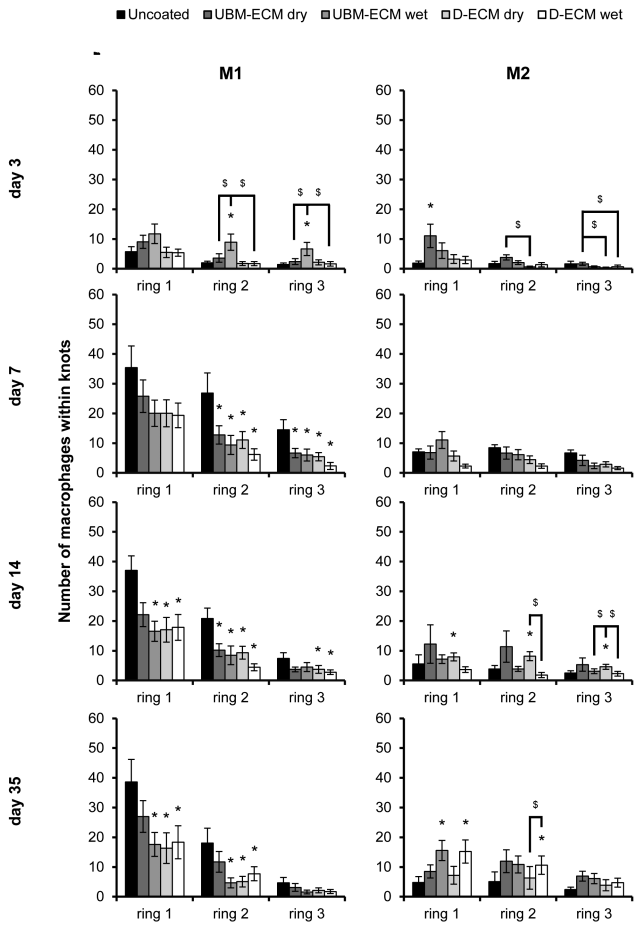

Figure 6.

Macrophage polarization within mesh fiber knots in uncoated and ECM hydrogel coated mesh. The number of M1 (CD86+/CD68+) and M2 (CD206+/CD68+) macrophages in response to uncoated, UBM-ECM dry coated, UBM-ECM wet coated, D-ECM dry coated, and D-ECM wet coated polypropylene mesh were quantified from high magnification images of implanted mesh within fiber knots. Total M1 and M2 macrophages were counted at each increasing distance interval from the mesh fiber surface (ring 1-3) at 3, 7, 14, and 35 day time points. Statistical significant differences were determined with ANOVA ($p < 0.05$) and denoted with (*) as different from uncoated mesh, or ($) as different between ECM coating groups.

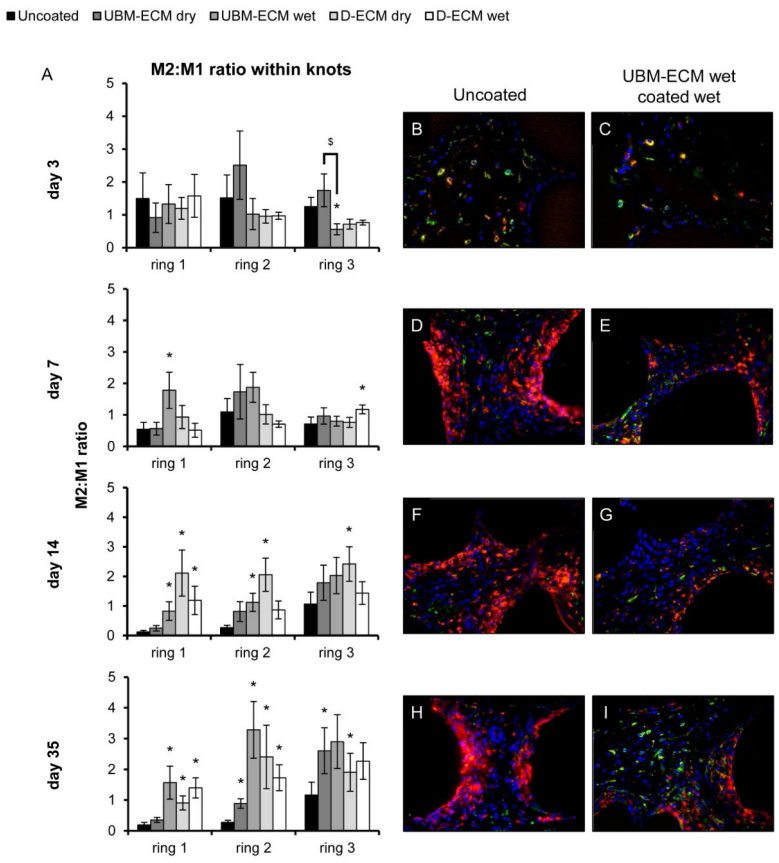

Figure 7.

M2:M1 polarized macrophage ratio within mesh fiber knots. The ratio of M2 to M1macrophages in response to uncoated, UBM-ECM dry coated, coated UBM-ECM wet coated, D-ECM dry coated, and D-ECM wet coated polypropylene mesh was determined for each distance (ring 1-3) from the mesh fiber surface at 3, 7, 14, and 35 days post implantation within fiber knot locations (A). Representative images of uncoated polypropylene mesh (B,D,F,H) and UBM-ECM wet coated mesh (C,E,G,I) are shown at each time point. Statistical significant differences were determined with ANOVA ($p < 0.05$) and denoted with (*) as different from uncoated mesh, or ($) as different between ECM coating groups. Scale bar represents100 μm.

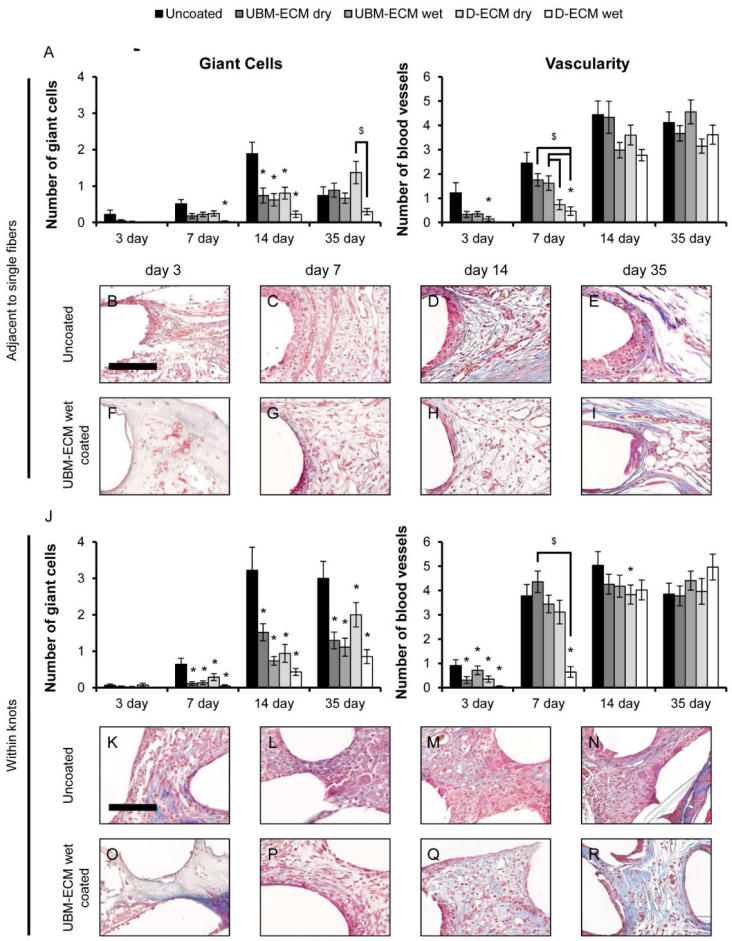

Figure 8.

Histologic remodeling response to uncoated and ECM hydrogel coated mesh. The total number of foreign body giant cells and blood vessels were quantified from high magnification (400X) Masson's Trichrome stained images adjacent to single mesh fibers (A) and within mesh fiber knots (J) after 3, 7, 14, and 35 days post implantation. Representative images of uncoated polypropylene mesh (B-E, K-N) and UBM-ECM wet coated mesh (F-I, O-R) are shown at each time point. Statistical significant differences were determined with ANOVA ($p < 0.05$) and denoted with (*) as different from uncoated mesh, or ($) as different between ECM coating groups. Scale bar represents100 μm.